Aqueous CdPbS quantum dots for near-infrared imaging

2012 Nanotechnology 23 275601

(http://iopscience.iop.org/0957-4484/23/27/275601)

Nanotechnology **23** (2012) 275601 (9pp) doi:10.1088/0957-4484/23/27/275601

Aqueous CdPbS quantum dots for near-infrared imaging

Giang H T Au[1], Wan Y Shih[1], S-Ja Tseng[2] and Wei-Heng Shih[2]

[1] School of Biomedical Engineering, Science and Health Systems, Drexel University, 3141 Chestnut Street, Philadelphia, PA 19104, USA
[2] Department of Materials Science and Engineering, Drexel University, 3141 Chestnut Street, Philadelphia, PA 19104, USA

E-mail: shihwh@drexel.edu

Received 19 February 2012, in final form 1 May 2012
Published 18 June 2012
Online at stacks.iop.org/Nano/23/275601

Abstract
Quantum dots (QDs) are semiconducting nanocrystals that have photoluminescent (PL) properties brighter than fluorescent molecules and do not photo-bleach, ideal for *in vivo* imaging of diseased tissues or monitoring of biological processes. Near-infrared (NIR) fluorescent light within the window of 700–1000 nm, which is separated from the major absorption peaks of hemoglobin and water, has the potential to be detected several millimeters under the surface with minimal interference from tissue autofluorescence. Here we report the synthesis and bioimaging demonstration of a new NIR QDs system, namely, CdPbS, made by an aqueous approach with 3-mercaptopropionic acid (MPA) as the capping molecule. The aqueous-synthesized, MPA-capped CdPbS QDs exhibited an NIR emission in the range of 800–950 nm with $x_i \geq 0.3$, where x_i denotes the initial Pb molar fraction during the synthesis. Optimal PL performance of the CdPbS QDs occurred at $x_i = 0.7$, which was about 4 nm in size as determined by transmission electron microscopy, had a rock salt structure and a quantum yield of 12%. Imaging of CdPbS QDs was tested in membrane staining and transfection studies. Cells transfected with CdPbS QDs were shown to be visible underneath a slab of chicken muscle tissue of up to 0.7 mm in thickness without the use of multiple-photon microscopy.

(Some figures may appear in colour only in the online journal)

1. Introduction

Quantum dots (QDs) are semiconducting nanocrystals with distinctive photoluminescence properties that are much brighter than traditional fluorescent molecules (fluorophores) and do not photo-bleach, an important attribute for disease imaging [1–4]. Specific antibody-bound QDs can be used to image antigens on cellular, endothelial, or mucosal surfaces *in vivo* [5]. For example, fluorescence of antibody-linked QDs bound to the cancerous tissues in a mouse helped locate the tumor [6]. In addition, cellular proliferation can be quantified using a QD-based incorporation assay [4]. QDs have also been illustrated in molecular beacons to detect DNA [7–9].

Most commercial QDs are made using an organometallic-precursor route in an organic solvent that is hazardous to the environment and to the health of the workers. These organic solvent-derived QDs must be transferred from the organic solvent to an aqueous medium for bioimaging application, which requires multiple steps of ligand and solvent exchange. It would be desirable—especially for bioimaging applications—if QDs could be synthesized in an aqueous approach so that the as-synthesized QDs could be directly applied for bioimaging without the need of tedious ligand and solvent exchange to minimize the potential hazard to the environment and human health. In our laboratory, we have developed an aqueous synthesis route that produces highly luminescent CdS QDs that are less than 5 nm in size and capped with 3-mercaptopropionic acid (MPA) in one single step that can be readily conjugated for bioimaging [10]. A similar aqueous approach also produced bright ZnS-based QDs [11–13]. It has also been shown that by first synthesizing ZnS QDs with MPA as the

capping molecule and subsequently replacing MPA with 3-mercaptopropyltrimethoxysilane (MPS), a quantum yield (QY) as high as 75% could be achieved with ZnS QDs [13].

Near-infrared (NIR) light within a spectral window of 700–1000 nm has a minimal overlap with the major absorption peaks of hemoglobin and water [14]. As a result, NIR light has the potential for deeper tissue penetration than visible light [15, 16]. For example, emission spectra centered at 840, 1110, 1320, and 1680 nm enable a detection depth of up to 5–10 cm [4, 15]. Recently, NIR QDs were demonstrated for direct infrared visual guidance throughout a sentinel-lymph-node mapping procedure in a pig, which had the potential to minimize incision and dissection inaccuracies as well as real-time confirmation of complete resection during surgery [17]. NIR QDs are also compatible with many infrared sensing and imaging technologies [18]. Moreover, NIR emission has minimal interference from tissue autofluorescence, which centers mostly around the green color (500–600 nm) [19]. Because of these benefits, much effort has been devoted to the development of NIR QDs [20]. InAs/InP/ZnSe and CuInSe/ZnSe (759 nm) NIR QDs with core/shell/shell or core/shell structures are examples of NIR QDs with the potential for deep-tissue imaging due to their longer wavelength and relatively low toxicity [21, 22]. The InAs(ZnCdS) NIR QDs have been conjugated with streptavidin for cellular imaging at a depth of up to 200 μm with multiple-photon microscopy [16]. However, these QDs were synthesized in an organic route that required multiple solvent- and ligand-exchange steps before they could be used for conjugation for imaging purposes. Here we report a new NIR QD system, CdPbS, obtained using an aqueous synthesis route and its demonstration in bioimaging applications.

2. Materials and methods

2.1. Cd and Pb precursor solutions

0.08 M Cd precursor solution and 0.08 M Pb precursor solution were prepared by dissolving 1.19 g of cadmium nitrate tetrahydrate $Cd(NO_3)_2$ (Alfa Aesar, MA) and 1.32 g of lead nitrate $Pb(NO_3)_2$ (Alfa Aesar, MA) in 50 ml of de-ionized (DI) water, respectively. The precursor solutions were stirred for 15 min at room temperature. The precursor solutions, which were then stored in the dark for later use, could be stable for several weeks. Note that all QD synthesis and processes were carried out at room temperature.

2.2. CdPbS synthesis

CdPbS QDs with an initial nominal molar fraction of Pb, x_i ranging from 0.1 to 0.9, were prepared as follows, where $x_i = [Pb]_i/([Cd]_i + [Pb]_i)$ with $[Pb]_i$ and $[Cd]_i$ being the initial nominal concentrations of Pb and Cd, respectively. First, 21 μl of MPA (molecular weight = 106 Da, density = 1.218 g cm^{-3}, Alfa Aesar, MA) was dissolved in 40 ml of de-ionized (DI) water and stirred for 10 min, followed by the addition of $(1 - x_i)$ ml of the 0.08 M Cd precursor solution and x_i ml of the 0.08 M Pb precursor solution. The solution was stirred for 10 min. The pH was then adjusted to 10.5 with tetramethylammonium hydroxide (TMAH), followed by the addition of 375 μl of 0.08 M Na_2S precursor (Sigma-Aldrich, MA). This would make the initial nominal MPA:$(Cd_{1-x_i}Pb_{x_i})$:S molar ratio 8:2.6:1. The solution was stirred for 10 min. Following the precipitation of CdPbS QDs, 2.4 mol excess Cd was added relative to each S and the pH was adjusted to 12 with TMAH to improve the PL intensity. The final nominal QDs concentration was 0.6 mM, based on the concentration of S. After the synthesis, the CdPbS QD suspension was kept at 4 °C overnight.

2.3. 3-mercaptopropyl trimethoxysilane (MPS) replacement

The suspension of MPA-capped CdPbS QDs was filtered using a 10 kDa filter (Amicon ultracel, Millipore, CA) by microcentrifugation at 3000 rpm for 10 min three times to remove excess MPA and unused precursors. In each filtering, 25% of the liquid in the suspension was removed. After each filtering, the volume of the suspension was brought back to initial value by adding DI water. In each MPS replacement procedure, 50 ml of the QDs suspension were used. The pH of the suspension was adjusted back to 12 before the addition of 5.6 μl of MPS (Sigma-Aldrich, MA). The suspension was then stirred continuously for 30 min. The nominal molar ratio of MPS:cations:S was 1:5:1. The MPS-replaced QD suspension was at 4 °C.

2.4. NIH 3T3 Cell culture and transfection experiment

NIH 3T3 was cultured with complete DMEM medium. The cell culture media contained 10% fetal bovine serum (FBS) and 1% penicillin–streptomycin. Cells were incubated at 37 °C with 5% CO_2 and split every 2–3 days. Polyethylenimine (PEI) (MW = 25 kDa, branched, Sigma-Aldrich, MA) was first diluted in a phosphate-buffered saline (PBS) solution at 1.43 mM. For transfection experiments, the MPS-replaced QDs were first filtered by microcentrifugation at 3000 rpm for 10 min three times to remove unbound MPS. Various amounts of the PEI solution ranging from 10 to 1000 μl were added to 1 ml of a 0.6 mM MPS-replaced CdPbS QDs suspension to achieve a PEI/QD number ratio of 1, 10, 20, 30, 50, 80, 100, 300, and 500 based on the QD particle concentration. The QD particle concentrations were estimated based on a QD size of 4 nm, as evident in the TEM and a lattice constant of 0.593 nm, which was calculated according to XRD pattern obtained in this study. Assuming the QDs to be cubes, a QD concentration of 0.6 mM based on S was equivalent to 0.733 μM based on QD particle concentration. For example, mixing 102 μl of a 1.43 mM PEI solution with 1 ml of a 0.6 mM QDs suspension (0.733 μM based on particle concentration) would yield a PEI/QD number ratio of 200. To maintain the same QD concentration at 0.366 μM by particle concentration for all PEI–QD mixtures, an appropriate amount of de-ionized water was added to bring the final volume to 2 ml. The pH of all PEI–QD mixtures was adjusted to 7 before transfection.

NIH 3T3 cells were transferred onto chamber slides and incubated in complete DMEM medium. After one day, the medium was replaced by a fresh medium. PEI–QD mixtures (20 μl) were added to the cell culture and incubated at 37 °C with 5% CO_2 for 24 h. Cells were then washed with PBS three times and fixed with 4% paraformaldehyde (EMS, Hatfield, PA) for 15 min, followed by washing again with PBS. 4′, 6-diamidino-2-phenylindole (DAPI) was added at the end to stain the nuclei.

2.5. Cell membrane imaging

To prepare the conjugated QDs, DSPE-PEG-Mal, 2000 (Creative PEG works, CA) was first dissolved in PBS at 10 mg ml^{-1}. Various amounts of DSPE-PEG-Mal solution were added to 1 ml of 0.733 μM (by particle concentration) MPS-capped QDs suspension. The DSPE-PEG-Mal/QD number ratios were 1, 10, 20, 100, and 200, based on the QD particle concentration. The final volume of all the mixtures was adjusted to 2 ml to ensure the same QD concentration of 0.366 μM by the particle concentration. NIH 3T3 cells were grown on chamber slides at 37 °C with 5% CO_2 for two days. The cells were then fixed with 4% paraformaldehyde and washed three times with PBS. No Triton X-100 or acetone was added to preserve the membrane characteristics of the cells. The DSPE-PEG-Mal QD mixtures were added to the chamber slides and incubated for 3 h at room temperature. The solution was removed and cells were washed with PBS three times. Finally, DAPI counter-stain was added.

The photoluminescence (PL) spectra were measured using a fluorometer (QuantaMaster 40, PTI, Birmingham, NJ). The x-ray diffraction patterns of the QDs were examined using a Siemens D500 x-ray diffractometer. The actual compositions between Cd and Pb in the QDs were measured by atomic absorption (AA) (AA240FS, Varian, Santa Clara, CA) spectroscopy. The absorption spectra were measured using a UV–vis spectrometer (USB4000, Ocean Optics, FL). The fluorescence images of the QDs were examined using an Olympus BX51 microscope with a NIR CCD camera (MicroVista, Intevac, CA). The size of the QDs was examined by transmission electron microscopy (JEM-2100, JEOL, West Chester, PA).

3. Results and discussion

Bulk CdS and bulk PbS have band gaps of 2.4 eV and 0.37 eV, corresponding to wavelengths of 517 nm and 3351 nm, respectively. This suggests that a NIR QD system is possible if Cd and Pb can both be incorporated in the QDs to form a solid solution. Here we show that indeed, under basic conditions (preferably at pH > 11), both Cd and Pb could be incorporated in the QDs and that the emission wavelength of the QDs changed with the Cd/Pb molar ratio. In the following, we use the 'initial' molar fraction of Pb, x_i, to denote CdPbS QDs of different Cd/Pb ratio. By varying x_i, we have examined the formation of CdPbS QDs and the resultant PL to identify the optimal x_i for NIR emission in the 700–1000 nm window. The formation of the CdPbS QDs and their resultant PL can be enhanced by the amount of MPA included in the initial precursor solutions and the amount of excess Cd^{2+} added after the initial precipitation of the QDs. A typical synthesis condition is characterized by the MPA:cations:S molar ratio among the MPA, the cations, namely Cd^{2+} and Pb^{2+}, and the sulfur in the solution. It was found that the optimal synthesis condition consists of having an initial MPA:cation:S molar ratio of 8:2.6:1 followed by adding 2.4 of excess Cd^{2+} to result in a final MPA:cation:S molar ratio of 8:5:1. In other words, there were 8 moles of MPA and 5 moles of cations for every mole of sulfur. Note that a similar PL enhancement by the addition of excess cations after the initial QD precipitation was also observed in ZnS and CdS systems [13, 23]. The final 'nominal' molar fraction of Pb, x_f, was related to the initial nominal molar fraction of Pb, x_i, as $x_f = (2.6/5)x_i = 0.52x_i$.

The PL spectra of the CdPbS QDs of various x_i were shown in figure 1(a). As can be seen, the PL emission spectra of the QDs with $x_i = 0.1$ and 0.2 peaked at around 500 nm, similar to that of CdS QDs [7]. In contrast, for $x_i \geq 0.3$, the PL emission peak shifted to the NIR range above 800 nm. The photoluminescence excitation (PLE) and the PL wavelengths of the CdPbS QDs versus x_i are shown in figures 1(b) and (c). There was an abrupt shift of the PL peak wavelength from around 500 nm for $x_i \leq 0.2$ to above 800 nm for $x_i \geq 0.3$. There was also a similar abrupt shift of the PLE wavelength above $x_i = 0.2$, although the up-shift of the PLE wavelength at $x_i = 0.2$ was not as drastic as that of the PL wavelength (figure 1(b)). These results indicate that at $x_i \leq 0.2$, the PL of the CdPbS QDs behaved like that of CdS, while at $x_i \geq 0.3$, a PbS-like behavior emerged (figure 1(c)).

The x-ray diffraction (XRD) patterns of CdPbS QDs for $x_i = 0.1$–0.9 were shown in figure 1(d). The XRD results for $x_i \leq 0.2$ exhibited the 110 and 220 peaks of a zinc blende structure, which is the structure of CdS [10]. For QDs with $x_i \geq 0.3$, the rock salt structure, which is the structure of PbS [24], began to appear and coexist with the zinc blende structure. Roughly in the range of $0.3 \leq x_i \leq 0.6$, both the zinc blende and the rock salt structure coexisted. To further clarify if the CdPbS QDs were solid solutions in the range of $x_i \leq 0.2$ and $x_i > 0.6$, we plot the position of the 220 peaks for both zinc blende and rock salt structures versus x_i in figure 1(e). According to Vegard's law [17], the lattice constant should vary linearly with the composition of the solid solution. In the range of $x_i \leq 0.2$, the solid solution behavior was evident by the shift of the 220 peak to a small angle due to the increase of the lattice constant by the increasing amount of Pb in the zinc blende structure. A similar decrease of the 220 peak position was also evident for $x_i > 0.6$, indicating a solid solution of the rock salt structure for $x_i > 0.6$. These XRD results indicate that the CdPbS QDs were crystalline solid solutions with a zinc blende structure at $x_i \leq 0.2$ and a rock salt structure at $x_i > 0.6$. For $0.3 \leq x_i \leq 0.6$, the QDs were a mixture of the zinc blende and rock salt structures. The abrupt transition in the PL behavior shown in figures 1(a)–(c) was well correlated with the structural change from the zinc blende structure of the CdS to the rock salt structure of PbS. The behavior of PLE shown in figure 1(b) indicates that, for $0.3 \leq x_i \leq 0.6$, the excitation wavelength is a linear combination of the zinc

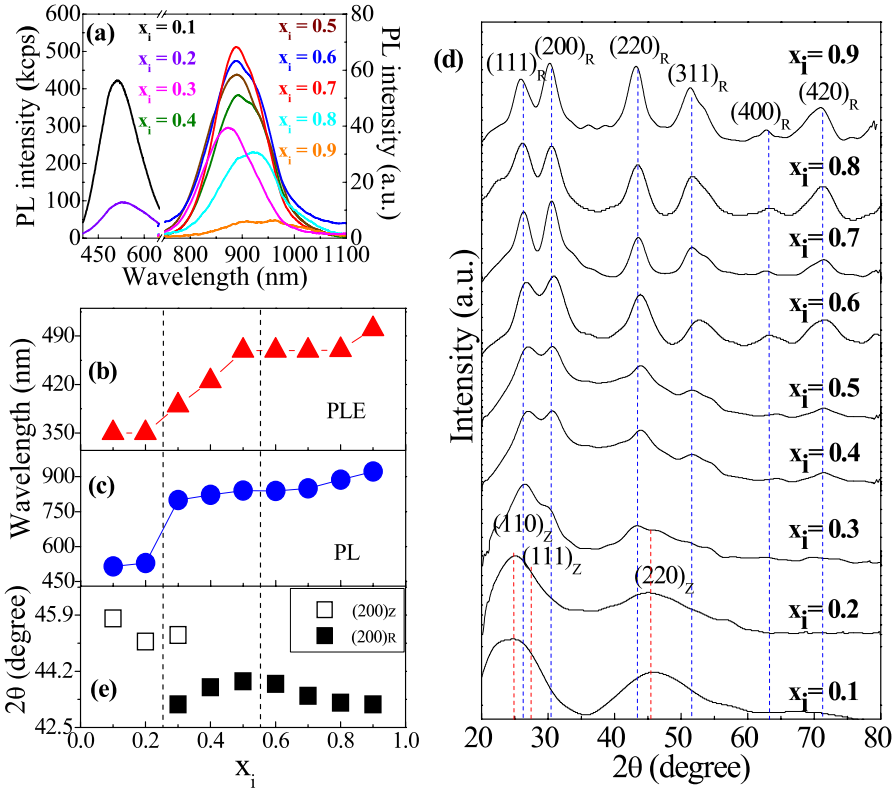

Figure 1. (a) Photoluminescence intensity of the QDs, the emission peak changed from 500 to 850 nm when $x_i \geq 0.3$ (b) PLE versus x_i; (c) PL versus x_i; (d) CdPbS obeys Vegard's law with respect to the $(220)_R$ peak; (e) XRD patterns evolve from zinc blende (Z) to rock salt (R) structure as the content of Pb, x_i, in CdPbS increases; blue dashed lines indicate rock salt peaks at $x_i = 0.7$, red dash-dotted lines indicate zinc blende peaks at $x_i = 0.2$.

blende and the rock salt phase, consistent with the XRD results shown in figures 1(d) and (e), only that the PL in the $0.3 \leq x_i \leq 0.6$ range seemed to be more dominated by the rock salt phase with an emission wavelength >800 nm. Further close spectroscopic examinations showed that all suspensions with $x_i \geq 0.3$ lacked emissions at around 500 nm, supporting the notion that the rock salt phase dominated the PL behavior. Note that the highest NIR emission intensity occurred at $x_i = 0.7$.

To determine the actual composition between Cd and Pb in the QDs we carried out atomic absorption (AA) spectroscopy studies. Before the AA measurement, the free Cd^{2+} and Pb^{2+} ions in the QD suspensions were removed by three repeated microcentrifugations with a 10 kDa filter, as described above. After each microcentrifugation, distilled water was added to bring the volume of the QDs suspension back to its initial value. The measured AA intensities for Pb and Cd were converted to concentrations according to the calibration curves. The result is shown in figure 2(a), where we plot the measured Cd and Pb concentrations versus the nominal concentrations of Cd and Pb. We denote the measured final molar fraction of Pb, x_m, where $x_m = [Pb]_m/([Pb]_m + [Cd]_m)$. The measured x_m (full squares) together with the nominal x_f (open circles) were plotted versus x_i in figure 2(b). As can be seen, the concentrations of the Cd and Pb incorporated in the QDs were lower than the initial nominal Cd and Pb concentrations, indicating that not all the Cd^{2+} and Pb^{2+} ions in the synthesis solution were incorporated into QDs. However, as shown in figure 2(b), the measured x_m final molar fraction of Pb incorporated in the QDs were quite similar to the nominal x_f for x_i up to 0.7. For $x_i \geq 0.8$, it was found that x_m was much larger than x_f, suggesting the Cd was harder to incorporate in the rock salt structure once the x_i exceeded 0.8. As a result, QDs with $x_i \geq 0.8$ exhibited a higher Pb molar fraction than the nominal value. It was known that excess Cd can improve the PL of the precipitated QDs [13]. We speculate that the PL intensity peak at $x_i = 0.7$ was related to the difficulty of incorporating Cd at $x_i \geq 0.8$.

Since the highest PL intensity was at $x_i = 0.7$, we focused the remainder of the study, i.e., QDs stability and bioimaging on the QDs with $x_i = 0.7$. The stability of the CdPbS QDs over time was evaluated by monitoring the quantum yield (QY) of the QDs over time. To measure the QY of the QDs, Rhodamine 101 (RD) (Fisher Scientific, Fairlawn, NJ) was used as the standard. Diluted RD solutions and QD suspensions were prepared. The absorption spectra of the diluted RD solutions and QDs suspensions were measured with the USB4000. The emission spectra were measured with the PTI with a common excitation wavelength of 460 nm. The integrated emission intensity and integrated absorption of each RD solution and each QD suspension were obtained by integrating the area under the emission peak and that under the absorption curve, respectively. The obtained integrated

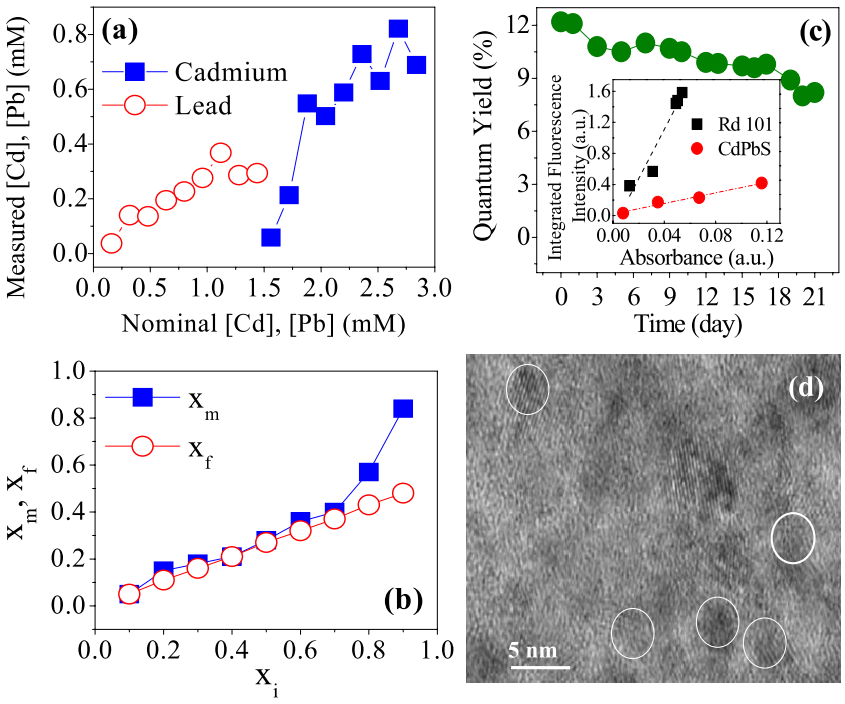

Figure 2. (a) Cadmium and lead concentrations measured by AA versus nominal cadmium (full squares) and lead concentration (open circles); (b) x_m and x_f versus x_i, where x_m, x_f, and x_i are as defined in the text; (c) quantum yield (QY) versus time; and (d) a TEM image of the CdPbS QDs with an $x_i = 0.7$. The inset in (b) is the integrated fluorescence intensity versus integrated absorption of the CdPbS QDs at $x_i = 0.7$ right after synthesis. The circles in (d) are to denote the QDs, whose size was around 4 nm.

emission intensity was then plotted versus the integrated absorption for both the RD and QDs. As an example, we show the integrated emission versus integrated absorption of the RD and the QDs of the first day in the inset of figure 2(c). With the QY of RD being 100% [25], the QY of the QDs could be obtained by dividing the slope of the integrated emission versus integrated absorption of the QDs by that of the RD as

$$\mathrm{QY} = \frac{\text{slope of QDs curve}}{\text{slope of RD curve}} \times 100\%. \qquad (1)$$

The QY of the CdPbS QDs versus time is shown in figure 2(c). As can be seen, the QDs had an initial QY of about 12% and retained a QY of about 8% even after 21 days of storing at 4 °C in the dark, indicating that the CdPbS QDs had a high QY and were stable over a long period of time.

A TEM micrograph of the CdPbS QDs is shown in figure 2(d), which shows the QDs to be about 4 nm and unagglomerated.

To test the utility of the CdPbS QDs at $x_i = 0.7$ in bioimaging, we show two examples. The first example is the transfection of MPS-replaced CdPbS QDs in the cytoplasm of mouse fibroblast cells NIH 3T3 (ATCC, Manassas, VA) using PEI as a carrier. MPS-replaced CdPbS QDs were used for better photo-stability and were obtained by the addition of MPS in the CdPbS QD suspension, as described above [11]. In the following, we refer to CdPbS QDs simply as QDs for simplicity.

For transfection, we first examined the size and charge of the PEI–QD complex at various PEI/QD number ratios 1, 10, 20, 30, 50, 80, 100, 200, 300, 500, 800–1000. We started all PEI–QD mixtures at a QD particle concentration of 0.366 μM, a volume of 2 ml, and an initial pH of 12. The mixtures were incubated at room temperature for 10 min. The suspension pH was then adjusted to 7 using nitric acid. PEI was positively charged in water due to the amine groups in the PEI. On the other hand, the MPS-replaced QDs were negatively charged due to the silanol and thiol of MPS. When the PEI/QD ratio increased, heterogeneous aggregation occurred due to the opposite charges carried by the PEI and the QDs [26]. The size and the zeta potential of the PEI–QD complex, as measured by the ZetaSizer (Malvern), versus the PEI/QD ratio are shown in figures 3(a) and (b), respectively. The PL intensity of the PEI–QD complex versus PEI–QD number ratio, as measured by the Tecan plate reader (Infinite 2000, Tecan, MA), was plotted in figure 3(c). At zero PEI concentration, the size of the QDs as measured by the ZetaSizer was around 3–5 nm (figure 3(a)), consistent with the 4 nm size obtained by TEM, and the zeta potential of the QDs was −25 mV (figure 3(b)). As we can see from figure 3(a), the size of the PEI–QD complex increased rapidly, exhibited a maximum of about 600 nm at a PEI/QD number ratio of around 10, decreased with further increase of the PEI/QD number ratio, and saturated at a size of about 30 nm at PEI/QD number ratios > 200. At the same time, the zeta potential of the complex increased sharply from negative to neutral at the PEI/QD number ratio where the PEI–QD complexes exhibit a maximal size. The size distribution of PEI/QD = 300 is narrow compared to the PEI/QD = 10 where the PEI formed big aggregate with the QDs. It indicates the complex was more stable at higher

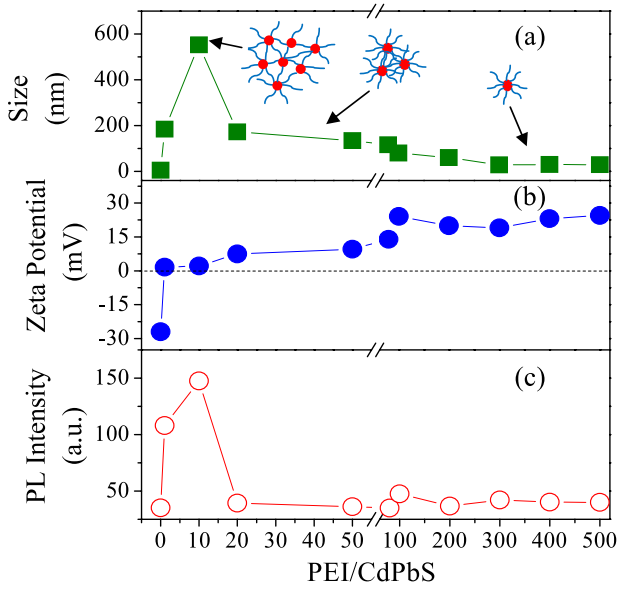

Figure 3. (a) Particle size of QDs as a function of PEI/CdPbS molar ratio. The maximum size was 550 nm at PEI/CdPbS = 10. The size decreased as the PEI/CdPbS ratio increased. The size reached the saturated point as PEI/CdPbS > 200. The PL intensity of all the complexes >50 was very similar to the non-conjugated QDs, suggesting a single QD with many PEI molecules on the surface. (b) Zeta potential of CdPbS QDs as a function of PEI/CdPbS molar ratio. The zeta potential changed to positive as the PEI/CdPbS ratio increased. The potential reached +25 mV as PEI/CdPbS > 200. This indicates the complex was stable as PEI/CdPbS > 200. (c) Photoluminescence intensity as a function of PEI/CdPbS molar ratio.

PEI/QD ratios, so that they were able to repel each other, whereas PEI/QD of lower ratios were not stable and formed aggregates of random pattern, resulting in large distribution in size. A further increase of PEI/QD ratio increased the positive charge of the complex, resulting in the breakup of the PEI–QD complex reducing its size. This kind of behavior is typical of systems where hetero-aggregation occurs [27, 28] and was also observed in the previous studies of CdS QDs with PEI [29]. A schematic of such heterogeneous aggregates is depicted near the peak of the PEI–QD size in figure 3(a). At large PEI/QD ratio > 200, the zeta potential of the PEI–QD complex was above +25 mV and its size was about 30 nm, suggesting that PEI–QD complexes may be thought of as sunflowers, with the QDs as the 'sunflower head' and the PEI as the 'petals' around the sunflower head, as schematically shown in figure 3(a). A schematic of such a 'sunflower-like' PEI–QD complex is depicted near the plateau above PEI/QD number ratio > 200. Note the size of an individual PEI was about 8 nm (data not shown) and that of the QD was about 4–5 nm. That the overall size of a complex was about 30 nm suggests that the adsorbed PEI on the QD surface was stretched outwardly due to the high PEI/QD ratios.

Figure 3(c) shows the PL behavior of the PEI–QD complex. One can see that as the PEI/QD ratio increased to 10, where the size of the PEI–QD complex exhibited a maximum, the PL intensity of the PEI–QD complex also exhibited a maximum. As the PEI/QD ratio increased to above 50, the PL intensity of the PEI–QD complex decreased and saturated at a value that was similar to that of QDs alone. Figure 3 shows that a larger PEI–QD complex has a higher PL intensity. The reason why a larger PEI–QD complex is brighter is unknown, and will be addressed in future study. That, at higher PEI/QD ratios, the PL intensity of the PEI–QD complex was similar to that of QDs alone was consistent with the notion that, under these conditions, QDs were well separated due to the PEI layer surrounding each QDs.

We tested the transfection performance of PEI–QD complexes of various ratios. PEI–QD complexes with a PEI/QD ratio of 300 showed the best transfection results, as judged by the intensity of the PL and the uniformity of the distribution of the PL inside the cells after transfection. As an example, we show a bright-field image, a DAPI image, a QDs image, and the overlap of all three of the same cells in figures 4(a)–(d), respectively. These four images together indicate that the PEI–QD complex was able to enter the cytoplasm and remain fairly uniformly distributed inside the cytoplasm. Although the present study could not provide the distribution of the QDs in the thickness direction to unambiguously indicate that the QDs were inside the cells, there was no fluorescence signal overlapping with the outlines of the cells. This indicates that the QDs were likely inside the cells rather than on the membrane surface. For the present study, we did not perform cytotoxicity test on the transfected cells, as our focus was more on the imaging of the NIR QDs. However, in our previous transfection study of CdS QDs to PC12 cells, we found that the toxicity of the PEI–QD complex was lower than that of PEI alone and cells were viable after transfection [29]. It is likely the present CdPbS QDs will behave similarly. More detailed CdPbS QDs transfection studies will be carried out in a future study.

The second bioimaging example was cellular membrane imaging using 1,2-distearoyl-sn-glycero-3-phosphoethanolamine-polyethylene glycol-maleimide (DPSE-PEG-Mal) conjugated QDs. The conjugated QDs were tested on both cells and paraffin-embedded breast tissue slides. The best ratio for DSPE-PEG-Mal/QD ratio was 50, as judged by the intensity of the PL and the uniformity of the distribution of the QDs on the cells. As an example, we show a bright-field image, a DAPI image, a QD fluorescence image, and the overlay of all three of the same cells treated with the DSPE-PEG-Mal–QD mixture at a DSPE-PEG-Mal/QD ratio of 50 in figures 5(a)–(d), respectively. As can be seen from figure 5(c), all cell membranes were uniformly stained by the QDs. In particular, the overlay in figure 5(d) clearly showed that the PL images of the QDs were contained well by the bright-field contour of the cells, indicating that the DSPE-PEG-Mal conjugated QDs were indeed capable of imaging cell membranes. We speculate that the DSPE part of the PEG mimics the tail of the phospholipids in the bi-layer of the cell membrane, with the maleimide reacting with the thiol of the MPS on the QD surface to covalently link to the QD. Confocal microscopy was used to determine whether the signal came from the QDs on the cell membrane or the internalized QDs in the cytoplasm (data not shown). A *z*-stack of the cells was obtained. A 3D surface plot was

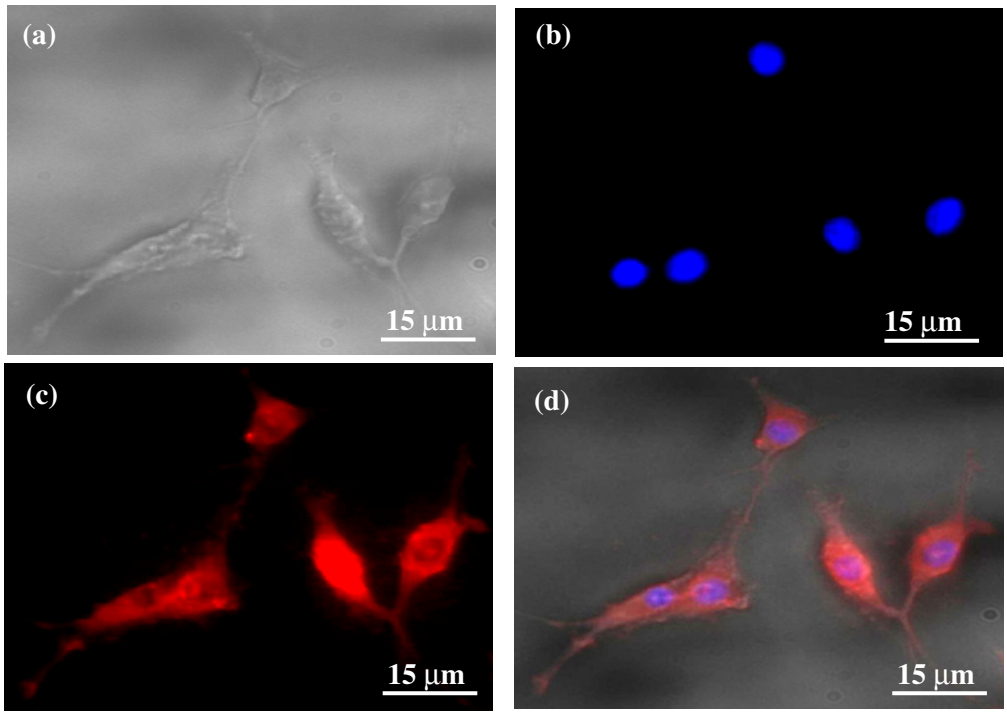

Figure 4. Fluorescence images of NIH 3T3 cells with transfected PEI–CdPbS QDs. (a) Bright field, (b) DAPI—nuclei, (c) PEI–CdPbS QDs, (d) overlay of bright field and fluorescence fields. The QDs were co-localized within the cytoplasm indicating QDs entered the cells through transfection.

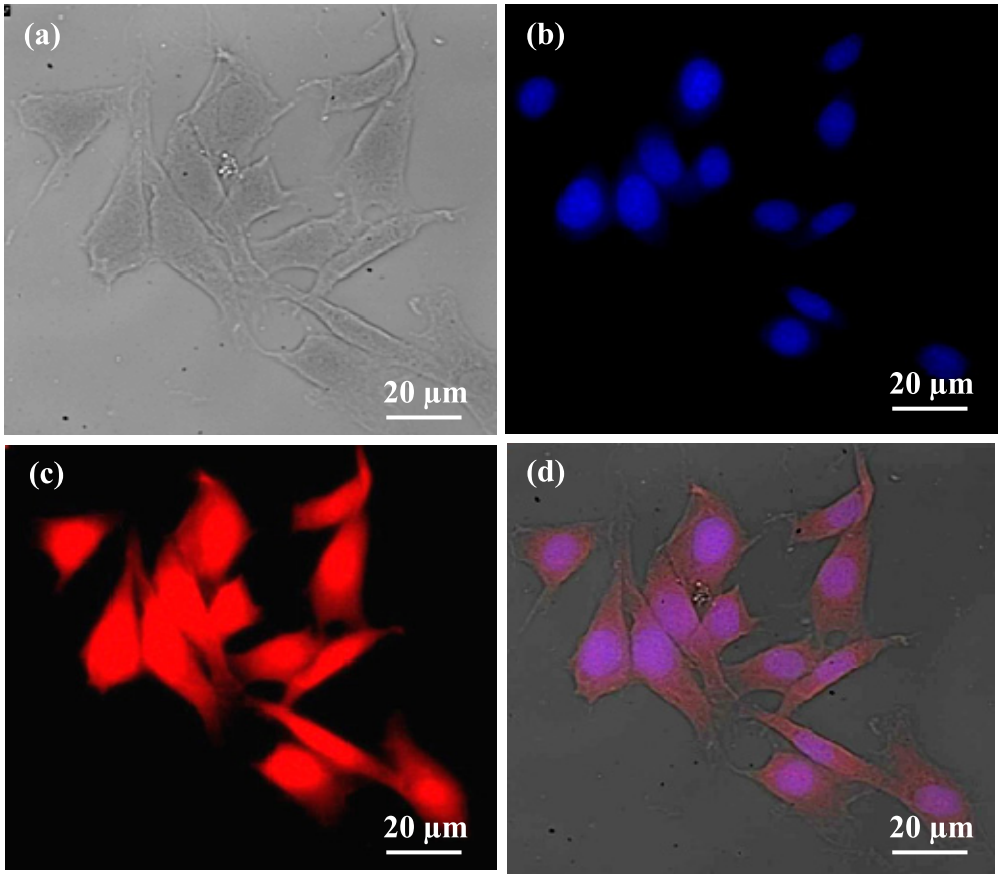

Figure 5. Mouse fibroblast NIH 3T3 membrane imaging using DSPE-PEG-Mal–CdPbS. (a) Bright-field, (b) DAPI—nuclei, (c) CdPbS QDs—cells membrane, (d) bright-field, DAPI and CdPbS QDs overlay. Signal was distributed evenly throughout the entire cells.

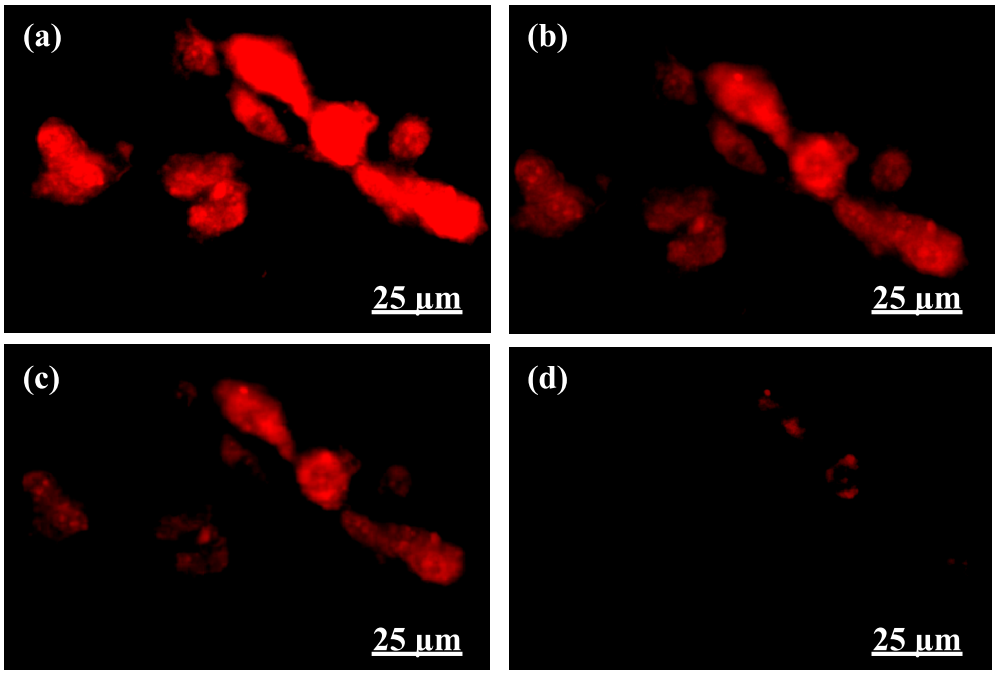

Figure 6. Tissue depth penetration capability of CdPbS QDs. Muscle laps were placed on top of transfected NIH 3T3 mouse fibroblasts. The maximum detection depth is around 0.7 mm. Penetration depths: (a) 0 mm, (b) 0.1 mm, (c) 0.4 mm and (d) 0.7 mm.

constructed at different depth, z. At the depth of the cell nuclei, there was no QDs emission. Emission was seen only at the bottom of the nucleus where the cell membrane was located. Furthermore, when moving away from the plane of nuclei, only the membrane of the cell was visible, and not the nuclei. This indicates that the designed DSPE-PEG-Mal conjugated QDs stayed on the cell membrane and not inside the cytoplasm.

To further examine the tissue penetration depth of the CdPbS QDs, fluorescence images of transfected cells were taken beneath layers of chicken muscle tissue of various thicknesses. The excitation intensity of the lamp was 13 mW mm^{-2}, with an image acquisition time of 270 μs. We show the fluorescence image of the same transfected cells alone, underneath 0.1 mm, 0.4 mm, and 0.7 mm thick chicken tissue in figures 6(a)–(d), respectively. As can be seen, the image of the transfected cells could be seen underneath a chicken muscle layer of up to 0.5 mm thick. The depth capability of the QDs was further analyzed using digitized images with ImageJ. The background fluorescence signal from the chicken tissues, although minimal, was subtracted from the QDs fluorescent signals from the fibroblast cells. We found that the QD-to-background contrast decreased with an increasing thickness of the chicken tissue with a maximal detection depth of about 0.7 mm due to microscope limitations. It is worth noting that the depth capability of the QDs shown above was achieved without the aid of multiple-photon microscopy.

It is of interest to note that, because the emission wavelength of the CdPbS QDs was well in the NIR range, imaging cells using the CdPbS QDs essentially removed the autofluorescence signal of cells. As a result, in a fluorescent microscopy session, the CdPbS QDs stained slides would appear pitch black to the human eye and only when the NIR CCD camera was switched on did a clear fluorescence image of the QDs appear on the computer screen. As an example, figure 7 showed that NIR QDs cannot be seen by naked eyes under a UV-lamp excitation whereas CdS QDs exhibited blue color under both a UV-lamp and fluorescence microscope. On the other hand, CdPbS QDs can be observed under an NIR CCD camera but not a UV-lamp. This indicates that the fluorescent image that we observed in the CdPbS QD system was due to the NIR emission of the CdPbS and the CCD camera could capture the NIR emission. This also indicates that imaging using the NIR CdPbS QDs can enhance the signal to noise ratio of the images as cellular and tissue autofluorescence were minimal in the NIR range.

4. Conclusion

In summary, we have successfully synthesized MPA-capped CdPbS QDs using an aqueous synthesis route under basic conditions, with initial Pb molar fraction (x_i) in the synthesis solution, followed by the addition of excess Cd^{2+}. It was shown that the measured final Pb mole fractions were similar to the nominal final mole fraction for $x_i \geq 0.7$. At $x_i \geq 0.3$, CdPbS QDs exhibited NIR emissions, with the optimal emission intensity occurring at $x_i = 0.7$ and a peak emission wavelength of 850 nm. These NIR CdPbS QDs were synthesized completely by an aqueous route that was different from the currently reported NIR system. The quantum yield at $x_i = 0.7$ was 12% and the XRD analysis showed that it was a solid solution in a rock salt structure. The imaging capability of CdPbS NIR QDs was demonstrated with membrane staining and transfection experiments. We

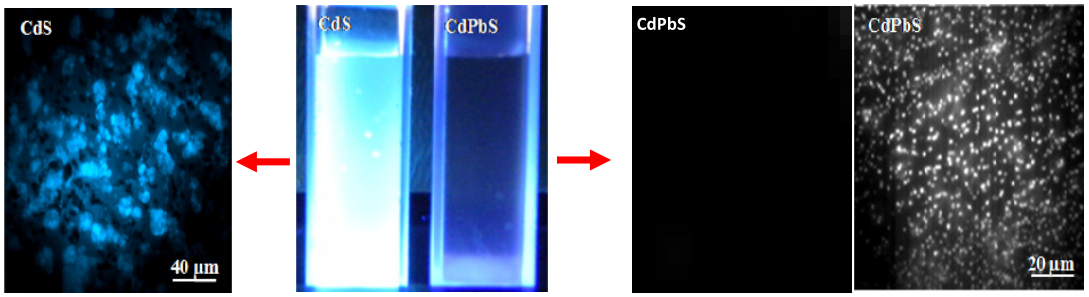

Figure 7. Under a UV-lamp, CdS QDs showed blue luminescent color whereas CdPbS QDs did not show any color due to the NIR range. A drop of QD suspension was placed on the glass slide surface and observed under a fluorescence microscope. When observed in the microscope, blue CdS QD dots were seen, but not CdPbS QDs. However, when the NIR CCD camera was turned on, bright dots were observed.

also demonstrated that the fluorescence of stained cells could still be observed under a slab of chicken tissue 0.7 mm thick without a confocal microscope. We believe that the current work will have a significant impact in the synthesis of new NIR materials as well as offering a new tool in tissue imaging.

Acknowledgments

We would like express our thanks for the support of Grants W81XWH-09-1-0701 from DoD and from Coulter Translational Research Partnership. S-Ja Tseng is grateful for the support of the National Science Council, Taiwan (NSC97-2917-I-007-102).

References

[1] Klarreich E 2001 *Nature* **413** 450–2
[2] Wu X, Lui H, Haley K N, Treadway J A, Larson J P, Ge N, Peale F and Bruchez M P 2003 *Nature Biotechnol.* **21** 41–6
[3] Gao X, Cui Y, Levenson R M, Chung L W K and Nie S 2004 *Nature Biotechnol.* **22** 969–76
[4] Obonvo O, Fisher E, Edwards M and Douroumis D 2010 *Crit. Rev. Biotechnol.* **30** 283–301
[5] Seydel C 2003 *Science* **30** 80–1
[6] Wu C S, Oo M K K, Cupps J M and Fan X 2011 *Biosens. Bioelectron.* **26** 3870
[7] Zhang C Y and Hu J 2010 *Anal. Chem.* **82** 1921–7
[8] Cady N C 2009 *Micro and Nanotechnology in Bioanalysis: Methods and Protocols* vol 544, ed J W Lee and R S Foote (Berlin: Springer) pp 367–79
[9] Kim J H, Chaudhary S and Ozkan M 2007 *Nanotechnology* **18** 195105
[10] Li H, Shih W Y and Shih W-H 2007 *Ind. Eng. Chem. Res.* **46** 2013–9
[11] Li H, Shih W Y and Shih W-H 2007 *Nanotechnology* **18** 205604
[12] Li H, Shih W Y and Shih W-H 2007 *Nanotechnology* **18** 495605
[13] Li H, Shih W Y and Shih W-H S 2010 *Ind. Eng. Chem. Res.* **49** 578–82
[14] Rogach A L and Ogris M 2010 *Curr. Opin. Mol. Ther.* **12** 331–9
[15] Allen P M, Lin W, Chauhan V P, Lee J, Ting A Y, Fukumura D, Jain R K and Bawendi M G 2010 *J. Am. Chem. Soc.* **132** 470–1
[16] Ntziachristos V, Ripoll J and Weissleder R 2002 *Opt. Lett.* **27** 333–5
[17] Kim S *et al* 2004 *Nature Biotechnol.* **22** 93–7
[18] Sargent E H 2005 *Adv. Mater.* **15** 515–22
[19] Yang M, Baranov E and Jiang P 2000 *Proc. Natl Acad. Sci. USA* **97** 1206–11
[20] He X, Gao J, Gambhir S S and Cheng Z 2010 *Trends Mol. Med.* **16** 574–83
[21] Xie R, Chen K, Chen X and Peng X 2010 *Nano Res.* **1** 457–64
[22] Park J, Dvoracek C, Lee K H, Galloway J F, Bhang H C, Pomper M G and Searson P C 2011 *Small* **27** 3148–52
[23] Hartnett P, O'Malley R, Shih W Y and Shih W-H 2009 *REU Poster* (Philadelphia, PA: Drexel University)
[24] Fernee M, Watt A, Warner J, Riches J, Heckenberg N and Rubinsztein-Dunlop H 2004 *J. Cryst. Growth* **270** 380–3
[25] Karstens T and Kobs K 1980 *J. Phys. Chem.* **84** 1871–2
[26] Denton A R and Ashcroft N W 1991 *Phys. Rev.* A **43** 3161
[27] Shih W Y, Shih W-H and Aksay I A 1996 *J. Am. Ceram. Soc.* **79** 2587
[28] Liu J, Sarikaya M, Shih W Y and Aksay I A 1990 *Phys. Rev.* A **41** 3206
[29] Li H, Shih W Y, Shih W-H, Chen L, Tseng S J and Tang S C 2008 *Nanotechnology* **19** 475101